MAE 5700 Final Report

Grace Falanga (gef45), Ben Inbar (bai8)

December 8, 2021

Member Contributions: Grace worked mostly on the heat conduction analysis, while Ben focused on the optimization of the wing design. We both collaborated on developing the approach, working through ANSYS issues, and the background research was split evenly.

Contents

1 Introduction

To this day there has only ever been one reusable human-rated space plane constructed and flown. NASA's Space Shuttles, which flew 133 successful missions, had a wide range of capabilities, from launching satellites to conducting repair work to hosting research projects, in part due to its unique design. The Shuttle would launch off of a rocket, but its wing design allowed it to act as a glider upon reentry, and it was created to be reusable [1]. After a series of safety issues resulting in tragic loss of life, in combination with high operational costs, the Space Shuttle program was retired in 2004 [2].

As human spaceflight is becoming more and more the "norm" that it seemed to be in the height of the Space Shuttle era, we were interested in understanding the loading on a space plane wing during reentry of the Earth's atmosphere. We decided to use the Space Shuttle profile as a starting point to design an optimized wing based on the results on finite element analysis (FEA) modeling of mechanical and thermal stresses during a typical reentry. In our design, our overall goal is to make the wing as lightweight as possible, as this would help to reduce mission costs or increase payload capabilities. Mass is a critical limiting factor in all spaceflight operations and so optimizing the structure while retaining its ability to handle reentry loading will be critical to any successful space plane. In order to do this, the variable components of our design are the thickness of the wing skin, spars, and ribs, the number of ribs and spacing, and the rib geometry.

An additional consideration in our design is the use of advanced materials available to us today that were not as developed during the Space Shuttle era. We aimed to investigate whether making the wing components out of aluminum or carbon fiber composite will provide better performance. For all of our simulations and calculations, we assume a carbon fiber-epoxy composite with a quasi-isotropic weave. We chose this weave, as its in-plane material properties are essentially isotropic. Along with this, we intended to model the thermal loading the exterior of the wing will be exposed to, and make an estimation for how thick a layer of insulation would be necessary as part of the wing skin. The thermal protection system is important throughout the entire space plane, but especially on the wings, which experience some of the highest temperatures during re-entry. On the Space Shuttle, the wing leading edge would experience temperatures upwards of 1600°C, so it is crucial to model and understand how to keep the actual wing components protected from these high temperatures [3]. In the case of an aluminum wing, this protection is even more critical due to the lower thermal performance of the metal compared to a carbon fiber composite part. In implementing a thermal protection system, the goal is to keep the wing parts from experiencing as much thermal loading as possible. We do recognize that the thermal protection system on the Space Shuttle and other space planes is more complex than a single layer of insulation, so we planned to make some simplifications in our model for the scope of this project.

While mass reduction is a priority, it cannot be at the expense of spacecraft survivability. Each of these components contributes in some way to survivability which creates a constraint

on the final design of the wing. The wing skin's TPS tiles, unlike on a regular aircraft, provides thermal protection against reentry heating and so must be sufficiently thick to prevent heating of the internal components of the wing. The spars and ribs must be able to bear the loads applied by hypersonic re-entry, and so the eventual configuration will be constrained by ensuring a low maximum wing tip deflection. This is critical because a high wing tip deflection could result in gaps opening up between thermal protection system tiles leading to catastrophic loss of vehicles as occurred in the Space Shuttle Columbia disaster [1]. Additionally, it is necessary to maintain the spaceplane's blunt body shape during reentry to prevent localized superheating; blunt bodies cause shockwaves to detach from the vehicles, preventing heating associated with attached shocks [4]. In order to maintain the blunt shape, the wings must not deflect significantly and thus must be stiffer than an ordinary aircraft. For our analyses, we have chosen a maximum wing deflection of 0.75% of the wingspan (9.2m), or 6.9 cm. By changing the thickness, spacing, and physical geometry of the spar and rib layout of the wing, we can find a low mass configuration that also meets our constraints.

In addition, we employed a factor of safety (FoS) of 1.4 for metallic components and 2.0 for composite components, when evaluating the maximum strength observed in our calculations, as per NASA standards for human spaceflight [5]. If the maximum calculated von Mises strength exceeded the material yield strength divided by the FoS (292 MPa for aluminum and 225 MPa for carbon fiber), we adjusted our design to ensure the wings meet required safety standards.

2 Approach

In our approach section we discuss the initial design of the wing and how the wing design was represented in ANSYS. We then discuss our approach for modeling both the thermal and mechanical loading of the wing. The thermal protection layer of insulating tiles does not add any structural support, and additionally the two problems have very different setups, so we modeled them in two separate steps. As will be discussed in Sections 2.2 and 2.3, we attempted to model 1D heat conduction, and 2D elasticity. Each of these setups required different numbers of degrees of freedom, which is dependent on the dimensionality of the problem as well as the given constraints or boundary conditions, which can take DOFs away.

2.1 Wing Design

NASA's Space Shuttle did not use a straight wing planform, instead using a double delta wing configuration due to the extreme heating that the standard straight wing was expected to experience (even greater than the re-entry heating encountered by the final design) [1]. We decided to use the double delta geometry of the Space shuttle as the base of our wing model. The inital internal geometry consisted of ribs and spars made of aluminum or carbon fiber composite and with an NACA 0012 airfoil shape. The NASA orbiters used a NACA 0012-64 airfoil which is a slightly modified NACA 0012 airfoil [6]. The general shape of the wing was

based on a high resolution CAD model of the Space Shuttle orbiter provided by the Johnson Space Center [7]. The initial internal geometry of the shuttle was be based off of technical drawings of the Space Shuttle, and then modified based on the results of our simulations [8]. The optimization process is described in more detail in Section 4.2.

2.2 Thermal Modeling

In our thermal modeling, we started by utilizing a few simplifications for the purpose of the scope of this project. We first only on the main portion of the wing skin, and ignored the wing tip. This is because the wing tip is the leading edge during re-entry, and is therefore exposed to significantly higher temperatures than the rest of the shuttle. As a result, the TPS on the wing tip was a reinforced carbon-carbon composite coating which could form to the contours of the wing and offer better protection for the extreme temperatures upon re-entry [1]. In our analysis, we will only looked at the main portion of the bottom wing surface, which utilizes a grid of 6-inch square, reusable thermally insulating tiles, and started by looking at a single tile's area. In the shuttle's designs, these tiles were placed on top of the aluminum wing skin, with a layer of strain isolation pad between, which prevented the brittle tiles from cracking as the ductile aluminum skin deformed [9].

In terms of insulating material for our design, we wanted to shift from the high-temperature reusable surface insulation (HRSI) used in the space shuttle, which were made of a silica ceramic component with a borosilicate glass coating. Instead, we decided to use an ultra-high temperature ceramic (UHTC), as they are more advanced materials and are able to withstand more extreme temperatures. For the purposes of this analysis, we are using a high-porosity UHTC, ZrB_2. It has a thermal conductivity, κ, of approximately 30 W/(m·K) and a heat capacity, C_p, of approximately 0.65 J/g·K at 750K. While both of these properties are dependent on temperature, in general, the thermal conductivity changes less than the specific heat, so we used a constant value of thermal conductivity. For heat capacity, we used representative values from a study investigating thermal properties of ZrB_2 to show change over temperature [10].

2.2.1 Equations

To determine the thickness of insulation required, we wanted to use a 1D heat conduction analysis, as almost all of the heat conduction was occurring in the direction perpendicular to the surface of the wing. However, since ANSYS is not capable of modeling 1D heat conduction we decided to use the axisymmetric approximation that was modeled in the homework for a cylinder. We are assuming that the temperature through each tile will not change along any direction except this perpendicular direction, so we felt the axisymmetric approach would be sufficient. The governing equation for this portion of our analysis was the 1D heat conduction equation, as shown in Eqn. 1.

$$\frac{d}{dx}(\kappa A\frac{dT}{dx}) + AQ = 0 \tag{1}$$

In this equation, which held for the width of the insulating tiles, the variable x represents the

direction of the thermal gradient, and we will assumed that the location where the insulation interfaces with the wing skin is $x = 0$. Q is the heat generation per unit volume, T is temperature, and κ is the material's thermal conductivity. As well, A is the surface area through which the heat is passing. Additionally, we took Q to be zero, because our internal wing components are not generating any heat. A schematic of our simplified model with the coordinate system used is shown in Fig. 1.

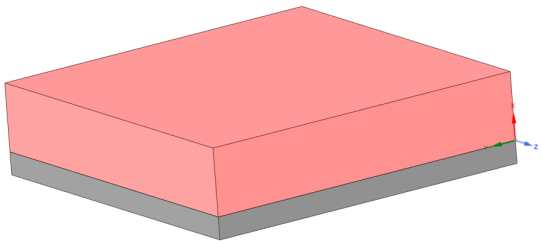

Figure 1: Schematic of a TPS for the area of a single tile, demonstrating the coordinate system used in thermal modeling. Grey region represents wing skin, while red region represents the insulating tile.

As detailed in Section 3.1, this initial approach was unsuccessful due to the way that we were specifying our boundary conditions, and resulted in us changing our approach. In doing so, we looked to the literature for a way to characterize the thermal loading in a transient model, as opposed to the steady-state thermal discussion we first attempted. We found a conference paper published by researchers at NASA Ames Research Center focusing on performing a finite element heat transfer analysis of the shuttle wing during re-entry [11]. In this paper, portions of the wing were modeled using NASA's FE analysis program, SPAR, and they utilized a transient thermal approach, instead of the steady-state approach we first attempted. For transient heat conduction, the right side of Eqn. 1 is no longer equal to 0, and instead has a time-dependent temperature term. This governing equation in 3D is defined in Eqn. 2 as

$$\kappa\left(\frac{\partial^2 T}{\partial x^2} + \frac{\partial^2 T}{\partial y^2} + \frac{\partial^2 T}{\partial z^2}\right) + q = \rho C \frac{\partial T}{\partial t} \tag{2}$$

where C is the material's specific heat.

With this new governing equation, we moved to a transient thermal setup in ANSYS, as opposed to the previous steady-state. In addition, we created a 3D model for the tile to use instead of a 2D representation. We then had to set up different boundary conditions that accounted for our transient thermal state. We started by extracting tabular data from the NASA article for temperature on the wing skin over time and using it as the boundary condition on the outer edge of the tile. The boundary conditions on the side remained the same (no heat flux), because our assumption that the tiles will have perfect insulators next to them did not change.

The final boundary condition, on the inside of the tile, was the most challenging to determine. As a rough approximation, we ended up using a convection boundary condition. We chose this

approximation because, in reality, there is a lot of radiative heat transfer occurring at the interface between the TPS and the aluminum body, which is quite difficult to model. By using the convection boundary condition, we can specify the temperature of the internal components that we want to maintain without setting it as a strict temperature boundary on the tile itself. As shown in Section 4.1, this allows us to see a difference in the internal temperature of the TPS as its thickness is changed, and permits us to make a determination of the thickness required.

2.2.2 Elements

In our initial heat conduction analysis, as mentioned above in Section 2.2.1, our ANSYS simulation was 2D-axisymmetric, so the elements were be 2-dimensional quadrilateral elements, giving us a linear temperature gradient in each element. After we adjusted our approach, since we switched to a 3D model we had solid elements instead. In inspecting the solution, we had 475 SOLID279 elements, which are 3D solid elements with 20 nodes each, and exhibit quadratic thermal behavior. Each node has a temperature DOF, and by having quadratic behavior, we can get a more accurate interpolation of temperature.

2.3 Mechanical Modeling

Additionally, we aimed to analyze the mechanical loading at 8 different altitudes as the shuttle reenters the atmosphere. We were primarily interested in how the wing bends in response to the aerodynamic loads it experiences, as well as ensuring that the maximum stresses in the wing do not cause serious deformation that could result in failure of the wing and loss of the vehicle. As mention in Section 1, it is crucial for plasma stability that the plane remain a blunt body, and any major deflection in the wing could risk sending shockwaves into the body.

2.3.1 Equations

In order to determine the bending and stress in the wing, we will use a 2D linear elasticity model. This model is adequate for our needs because we are not particularly interested in stresses occurring in the thickness direction since the thickness of all components of the wings is not significant compared to its other dimensions. We are concerned with the bending and stresses in the planar dimensions of the element which will be much greater due to the loading case. The governing equations for this analysis are shown in Eqn. 3 and 4.

$$\frac{\partial \sigma_{xx}}{\partial x} + \frac{\partial \tau_{xy}}{\partial y} = 0 \tag{3}$$

$$\frac{\partial \tau_{xy}}{\partial x} + \frac{\partial \sigma_{yy}}{\partial y} = 0 \tag{4}$$

In these equations σ_{xx} and σ_{yy} represent the are the normal stresses on the x or y faces in the x or y direction. τ_{xy} represents the shear force on the element. Additionally in order to

solve these equations, it is necessary to specify the stress-strain relationships shown in Eqn. 5.

$$\begin{aligned} \sigma_{xx} &= \frac{E}{1-\nu^2}(\epsilon_x + \nu\epsilon_y) \\ \sigma_{yy} &= \frac{E}{1-\nu^2}(\epsilon_y + \nu\epsilon_x) \\ \tau_{xy} &= \frac{E}{2(1+\nu)}\gamma_{xy} \end{aligned} \tag{5}$$

In Eqn. 5 E is the Young's Modulus of the material, ν is the Poisson's Ratio of the material, ϵ_i is the strain in the i direction, and γ_{xy} is the shear strain of the element. The strain-displacement relationships shown in Eqn. 6 are the other supplemental equations necessary to solve this problem.

$$\begin{aligned} \epsilon_x &= \frac{\partial u}{\partial x} \\ \epsilon_x &= \frac{\partial v}{\partial y} \\ \gamma_{xy} &= \frac{\partial u}{\partial y} + \frac{\partial v}{\partial x} \end{aligned} \tag{6}$$

In Eqn. 6 u and v represent the displacements in x and y respectively.

As briefly mentioned in Section 1 we investigated both aluminum and carbon fiber composite as materials for the internal structure of the space plane wing. Aluminum is a tested and proven material and was to create the internal structure of the NASA Space Shuttle [1]. Carbon fiber composites have not been used in this application before however there is precedence for using this material to construct a wing. The Boeing 787 Dreamliner is the poster child for carbon composite use in the aerospace industry composed of 50% composites by weight [12]. Composites are a significantly more mature technology than they were in the late 60s and early 70s when the Space Shuttle was being developed and they could lead to potentially significant weight savings.

2.3.2 Elements

In order to analyze the structural deformation of the wing, we will implement shell element mesh on our model. Shells were chosen because the thickness of the components are significantly smaller than the other dimensions. Shell elements allow us to set the thickness, but use a CAD model of our system that only represents the mid-lines of the components.

In the ANSYS meshing tool, SHELL181 elements were implemented in our mesh. These elements are 4 node quadrilateral elements with 6 degrees of freedom at each node but can be limited to 3 degrees of freedom by selecting membrane instead of membrane and bending as a stiffness option in ANSYS [13].

3 Analysis

3.1 Thermal Modeling

To perform the thermal analysis, we started by creating a geometry in SpaceClaim to represent the cross-section of the wing skin for one single TPS tile. We framed our geometry with the coordinate system shown in Fig. 1, where the origin starts at the interface between the wing skin and the TPS tile. This coordinate system was chosen to allow for easy analysis of the temperature gradient across the width of the insulation, enabling a determination for how thick the insulation needed to be. In following our original plan as explained in Section 2.2.1, we implemented a temperature boundary condition at $x = t$, where t is the thickness of the insulation that we are optimizing for. This edge will have a temperature of 1260°C, representing the upper temperature limit the wing would be exposed to [1]. The top and bottom edges (representing the boundaries where TPS tiles border one another) are considered to be perfect insulators, with a flux boundary condition of $\frac{\partial T}{\partial x} = 0$. Since we want to probe the temperature at $x = 0$, we set no boundary condition along the left edge. As seen in Fig. 2, these BCs are not correct, due to ANSYS automatically setting a temperature flux of 0 across any boundaries that are unspecified. As a result, the material acts as a perfect insulator and maintains uniform temperature across the entire piece.

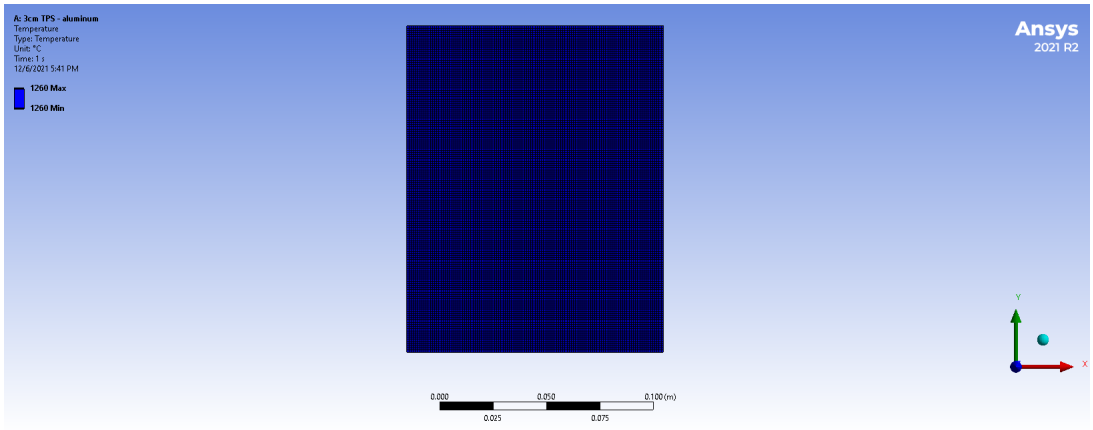

Figure 2: Results of ANSYS Steady-State Thermal modeling of TPS tile with a single temperature boundary on the right side ($x = t = 12$cm) of 1260°C

Once we realized that our setup was incorrect, we also came to realize that what we were trying to model was really heat flux, not heat conduction. Due to the simplicity of the geometry and our assumption of 1D conduction only, the problem becomes a very simple hand calculation for heat flux, q, across a boundary, as defined in Eqn. 7,

$$q = -\kappa \frac{dT}{dx} \tag{7}$$

with heat flux measuring heat transferred per area. We can easily complete this hand calculation

by completing the following integration in Eqn. 8,

$$\begin{aligned} qdx &= -\kappa dT \\ \int_{x=0}^{x=t} qdx &= -\int_{T=T_{in}}^{T=1260} \kappa dT \\ qt &= -\kappa(1260 - T_{in}) \\ t &= -\frac{\kappa(1260 - T_{in})}{q} \end{aligned} \tag{8}$$

where T_{in} is the internal temperature limit. This limit is dependent on material, so for the aluminum used on the original shuttle, T_{in}=176°C, and for a carbon fiber composite, thermal degradation starts at approximately 400°C[14]. At this temperature, in an oxidizing environment, oxidation starts to occur which will eventually cause the material's strength to decrease. As a result, we feel confident that using a limiting temperature of T_{in}=375°C in our thermal modeling will sufficiently represent protection of the system from thermal degradation.

We take the temperature at $x = t$ to be 1260°C, as this is the upper temperature limit for the shuttle. For q, we used the highest heat flux value reported in the NASA thermal FE simulations, which was -1.15 $\times$ 10^5 W/m^2. Using these values, we calculate that for aluminum, $t = 0.566$ m and for carbon fiber $t = 0.462$ m. As is discussed in Section 4.1, these thicknesses are definitely not the ideal case, but with the limited information on other material properties for UHTCs, we settled on ZrB_2 for a "proof of concept".

Using the hand calculations as a basis, we started with an initial thickness of 0.566 m for the aluminum case. We used the automatically generated mesh, as we are only interested in the final internal temperature, and we are treating the TPS tile as isotropic. As shown in Fig. 3 below, this initial guess leaves us with a maximum internal temperature of 343.89°C. In Fig. 4, we see the initial hand calculations result in a maximum internal temperature of 451.31°C. Since both of these temperatures are above the limits for their respective internal wing structure materials, in Section 4.1 we describe the process for how we optimized the thickness, protecting the internal components from any thermal stresses.

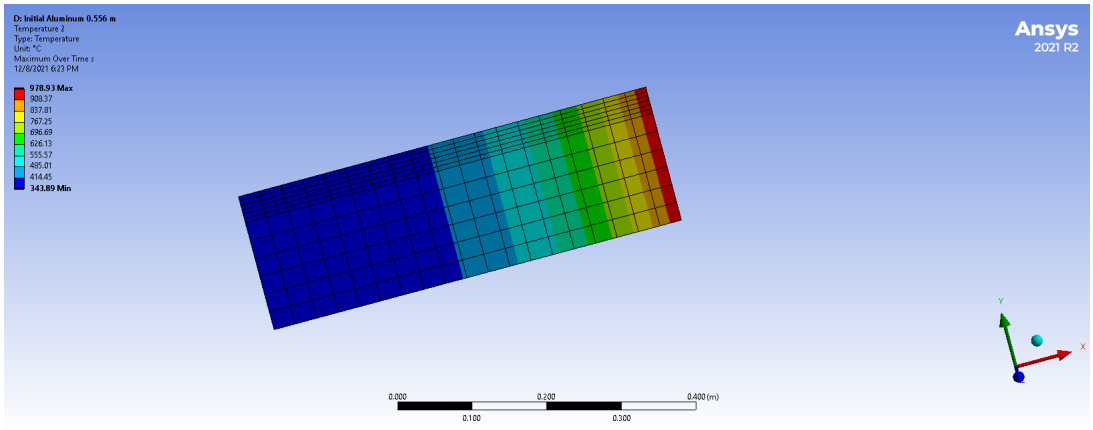

Figure 3: Results of ANSYS Transient Thermal modeling of a 0.566 m thick TPS tile with a time-varying temperature boundary on the right side, and a constant air convection boundary condition on the left side.

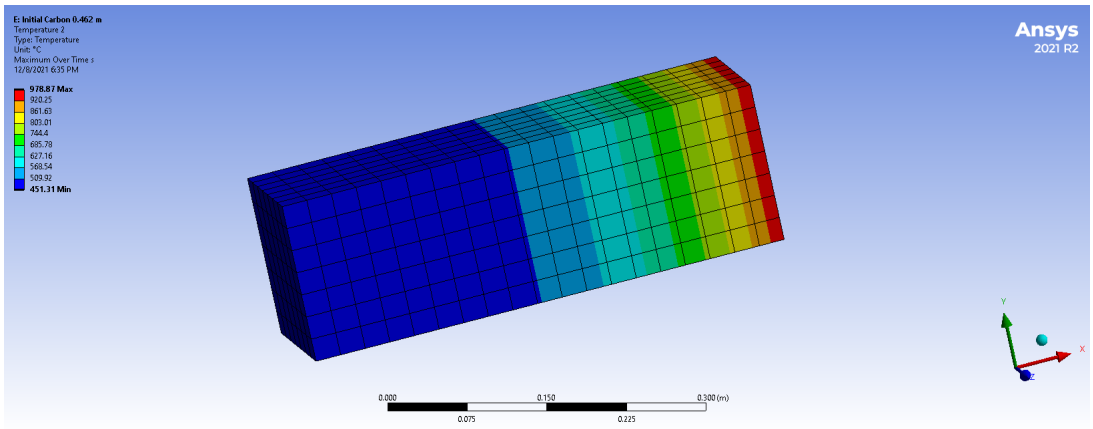

Figure 4: Results of ANSYS Transient Thermal modeling of a 0.462 m thick TPS tile with a time-varying temperature boundary on the right side, and a constant air convection boundary condition on the left side.

3.2 Mechanical Loading

To perform the mechanical analysis, we set up a model of the wing as described in Section 2.3. We applied a fixed boundary condition to the wing at the root where it joins to the fuselage of the vehicle. In order to determine the force applied to the wing by reentry we selected 8 representative altitudes over the course of the re-entry phase of the shuttle descent, for which we will analyze the loading on the wing. It is useful to define a body-fixed frame R_b centered at the vehicle center of mass with the direction x_b taken to be the direction from the center of mass to the nose, y_b taken to be the orthogonal vector in the direction of the wings, and z_b as direction orthogonal to the plane created by x_b and y_b in the direction that completes the right handed triad. The force on the wings will be due to the dynamic pressure experienced during reentry, as well as the low pressure zone created by the turbulent flow around the wings.

By applying this load to the wings and probing total deformation and von Mises stress we will determine if our current layout of wing components meets our requirements. If it does, we can then go on to optimize the layout to minimize the mass of the wing.

We chose to use a dynamic pressure profile given in Dr. John C. Adam's overview of atmospheric reentry as well as a 0^{th} order approximation for the low pressure generated by the turbulent flow to approximate the aerodynamic loads on the wing [15]. Table 1 shows the pressures exerted on both the top and bottom of the wing, with the bottom pressures corresponding to the dynamic pressure profile.

Table 1: Dynamic pressures on the top and bottom of the Space Plane wing [15]

Pressure (Pa)		
Bottom of Wing	Top of Wing	Altitude (km)
4731.9047	-8517.4285	30.594
5081.9176	-9147.4517	38.108
5162.6898	-9292.8416	43.036
5129.0347	-9232.2625	45.720
4987.6834	-8977.8301	49.672
4570.3603	-8226.6486	54.552
3816.4865	-6869.6756	60.895
1103.8867	-1986.9961	76.314

Calculating the top wing pressure would have required a complex and extensive computational fluid dynamics simulation of flow around the wing. Instead, under the advice of Dr. Perrine Pepiot, we chose to get an order of magnitude approximation by using established correlations for the pressure in the separated region of flow around a square cylinder. Using results for the coefficient of pressure at a wide spread of Reynolds numbers we were able to write a script that calculated an approximate pressure in the region above the top of the wing. Rearranging Eqn. 9 and using the relation that dynamic pressure $q \equiv p - p_\infty$ where p is the static pressure and p_∞ is the ambient pressure, we were able to solve first for V_∞ using $C_p = 1$ and then solved for the $p - p_\infty$ using $C_p = -1.8$ [16].

$$C_p = \frac{p - p_\infty}{\frac{1}{2}\rho_\infty V_\infty^2} \tag{9}$$

In following procedure laid out in Section 2.3.2, we applied the pressures to the wing geometry and fixed the wing root as the support. No other supports were necessary as the wing is only affixed to the orbiter at the root. We first conducted the analysis using Aluminum 2024-T36 as the airframe material. Fig. 5 shows the results of this first analysis. The optimization process is described in Section 4.2.

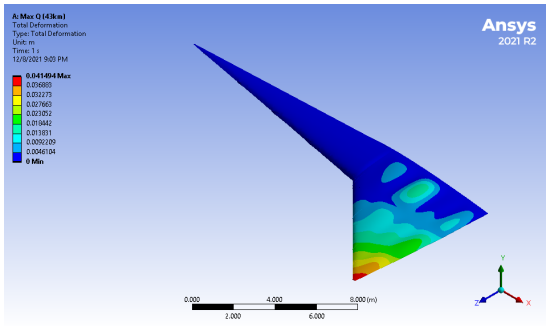

(a) Deformation of unoptimized airframe

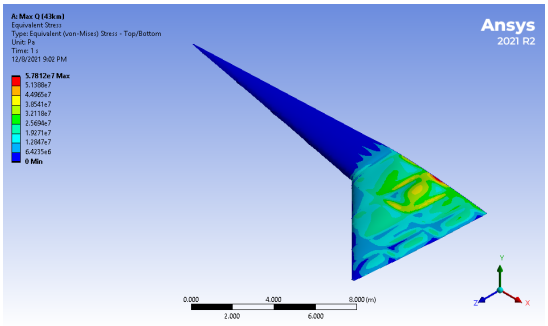

(b) Von Mises stress in unoptimized airframe

Figure 5: Initial results of simulated aerodynamic loading on a space plane wing. These results have not been optimized for weight however they do meet the criteria for stress and deformation as described in Section 1

4 Optimization

4.1 Thermal Modeling

Once we had a way to model the heat conduction through the TPS tile in ANSYS, at least to an order of magnitude, we started working on optimizing the thickness. The process for both scenarios (aluminum or carbon fiber wing components) was essentially the same, the only differences being the temperature requirement on the inner face of the tile and the temperature of the convection boundary condition, which corresponded with that limit. After realizing the thicknesses that resulted from the hand calculations would not be sufficiently thick given our simplifications and ANSYS setup, as described in Section 3.1 we first started by almost doubling the thickness, to hopefully get an overestimate. This was successful for both cases, with the aluminum wing system reaching 174.48°C, and the carbon system reaching only 78.85°C, as depicted in Fig. 6 and Fig. 7.

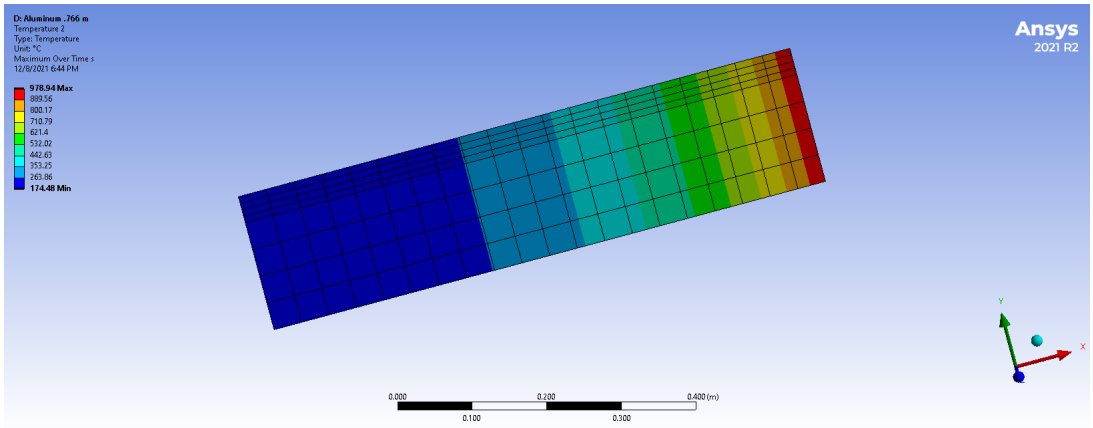

Figure 6: Results of ANSYS Transient Thermal modeling of a 0.766 m thick TPS tile with a time-varying temperature boundary on the right side, and a constant air convection boundary condition on the left side.

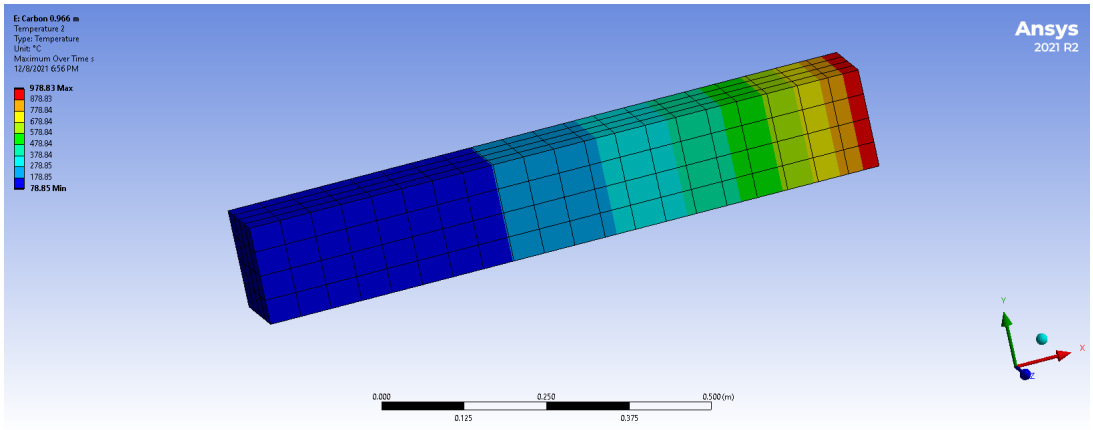

Figure 7: Results of ANSYS Transient Thermal modeling of a 0.966 m thick TPS tile with a time-varying temperature boundary on the right side, and a constant air convection boundary condition on the left side.

We then used an iterative process to change the thickness in SpaceClaim, update the geometry in ANSYS Mechanical, and re-solve the transient thermal problem. After overshooting and undershooting, we eventually were able to optimize the thickness for both cases to be as thin as possible, while still protecting the material against thermal degradation. In the end, our final designs are seen in Figures 8 & 9. For a wing made out of aluminum, with our estimates, it would require each tile to be 0.762 m thick. If, however, the plane is made from carbon fiber composite, each tile would only need to be 0.549 m thick.

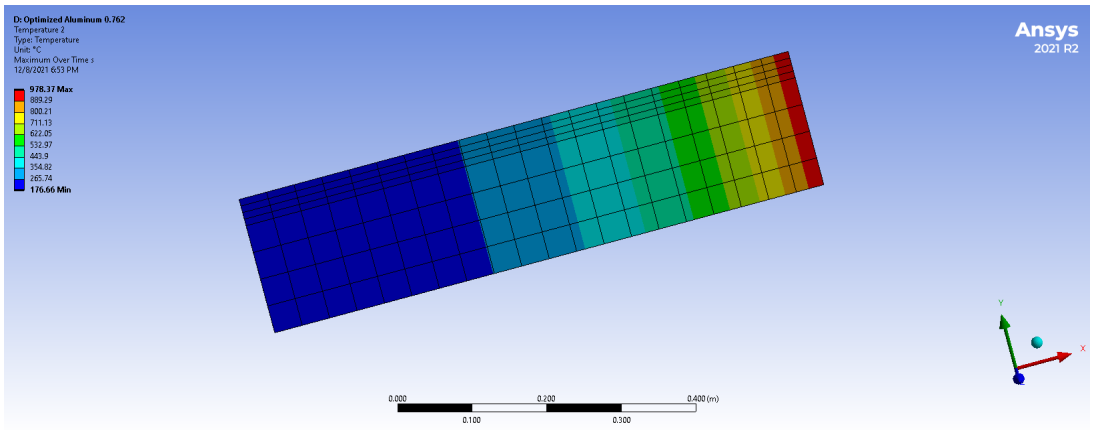

Figure 8: Results of ANSYS Transient Thermal modeling of a 0.762 m thick TPS tile with a time-varying temperature boundary on the right side, and a constant air convection boundary condition on the left side. Results represent the optimized thickness for an aluminum wing body.

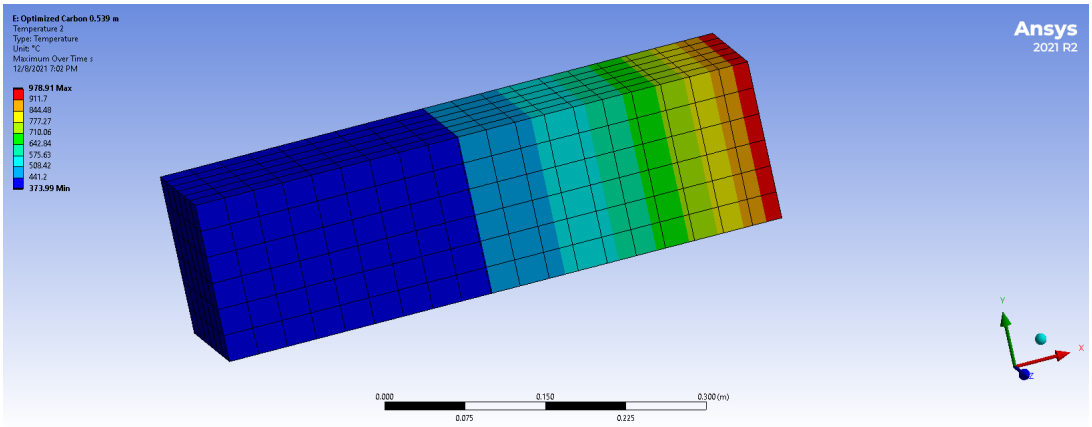

Figure 9: Results of ANSYS Transient Thermal modeling of a 0.539 m thick TPS tile with a time-varying temperature boundary on the right side, and a constant air convection boundary condition on the left side. Results represent the optimized thickness for a carbon fiber composite wing body.

Given the density of ZrB_2 to be approximately 6.085 g/cm^3 [10], each tile for the aluminum system would be 108 kg, and 77 kg for the carbon system. While immediately it is clear that the carbon system reduces a significant amount of weight (30 kg per tile), it is also important to recognize that this TPS would never actually go on a shuttle wing. Alternative materials must be considered, as will be discussed in Section 5, because otherwise the TPS would be too heavy to fly.

4.2 Mechanical Loading

To optimize the mechanical loading on the space wing, we focused on the structural design, namely the number of ribs and spars, their spacing, and the thicknesses of the ribs, spars, and skin (not including the thermal protection system). We started with a baseline design, and used the results to inform our optimization process. We used the same baseline geometry for both the aluminum and carbon fiber airframe and the optimization process in both cases was identical. Additionally, all analysis was conducted at re-entry Max Q (or maximum dynamic pressure) where there is the greatest force on the airframe which as shown in Table 1 occurs at an altitude of 43 km.

Fig. 5 shows the results of the aluminum baseline analysis, which produced very favorable results with a maximum stress of only 57.8 MPa and tip deflection of 4.15 cm. This indicated that our baseline geometry contained more than material than required and allowed us to begin removing structural components to reduce weight.

It was clear from the initial analysis that the forward portion of the wing was experiencing very little deflection or stress, allowing us to remove forward ribs and spars until the wing was lighter but still well supported. Fig. 10 shows the final internal geometry of the aluminum wing. The number of spars was reduced from 5 to 3 in the forward wing and the spars in the main delta were reduced from 5 to 4. Additionally the wing skin was able to be made very thin, with

the forward delta being only 3 mm thick, and the main delta having a wing skin thickness of 7.2 mm. All wing ribs and spars were able to be reduced in width only 2 cm each.

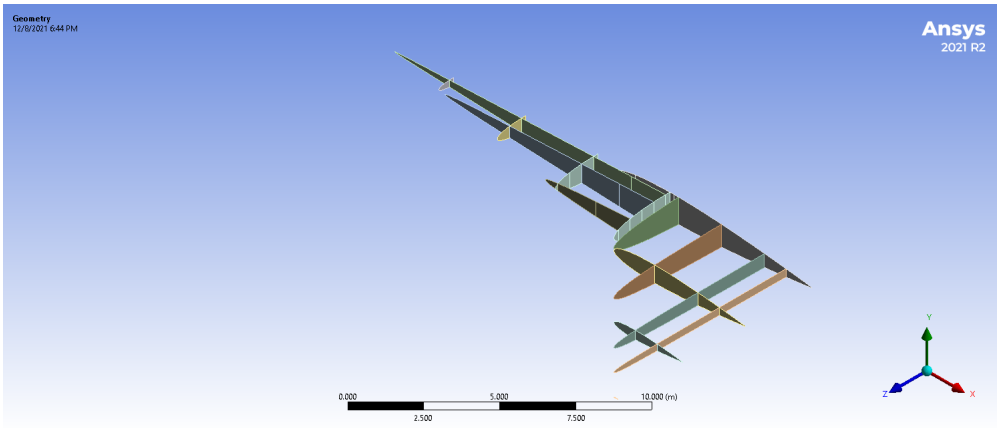

Figure 10: Internal geometry of final aluminum airframe. Wing skin has been hidden to allow viewing of ribs and spars.

The results of this optimization were higher stress and tip deflection than the base case, but still within the requirements. The results of the aluminum airframe optimization are shown in Fig. 11, and show that while the stress is still well below the maximum allowable stress, tip deflection is right below the .75% of span limit.

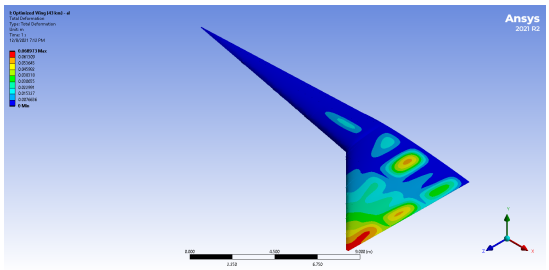

(a) Deformation of optimized aluminum airframe

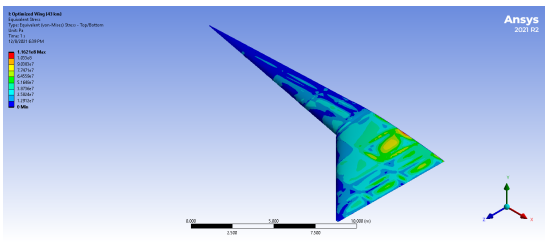

(b) Von Mises stress in optimized aluminum airframe

Figure 11: Results of simulated aerodynamic loading on a space plane wing. Have been optimized for weight and meet the requirements for stress and deflection outlined in Section 1

The same process was then carried out for the carbon fiber airframe. Unlike the aluminum frame, the baseline geometry did not immediately meet the requirements for tip deflection. To address this, a spar was added towards the trailing edge of the main delta wing, and the main delta wing's skin was thickened slightly. Once we had a passing geometry however many of the same changes were made to the geometry, including removing many of the same elements from the forward section of the wing. The final internal geometry of the carbon fiber wing is shown in Fig. 12

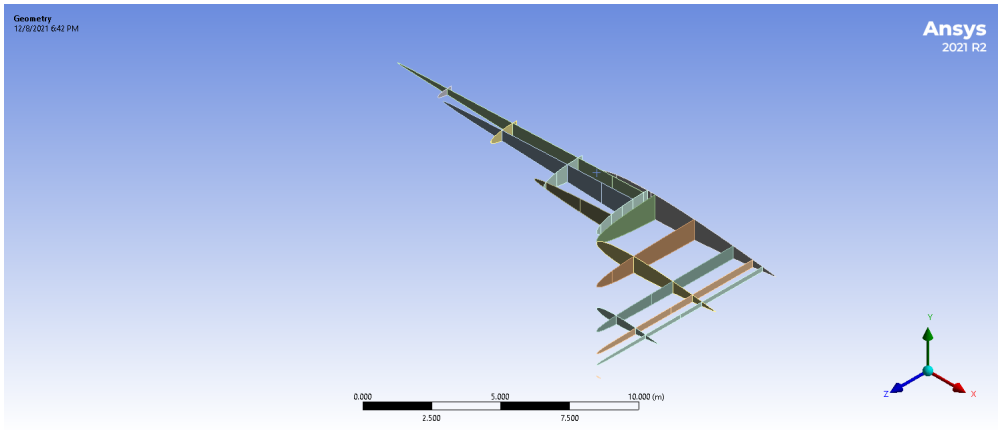

Figure 12: Internal geometry of final carbon fiber airframe. Wing skin has been hidden to allow viewing of ribs and spars.

The final wing design has a main delta wing skin thickness of 1.29 cm, and a forward delta wing skin thickness of 5 mm. The ribs and spars are all 2 cm thick, except for the three spars at the trailing edge which are 5 cm thick. Fig. 13 shows the final analysis of the deformation and stress on the wing.

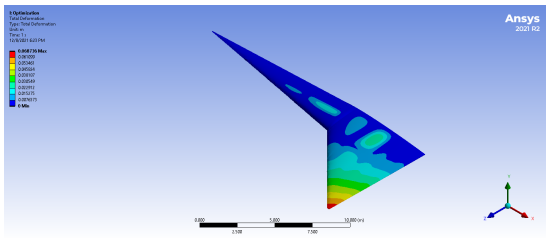

(a) Deformation of optimized carbon fiber composite airframe

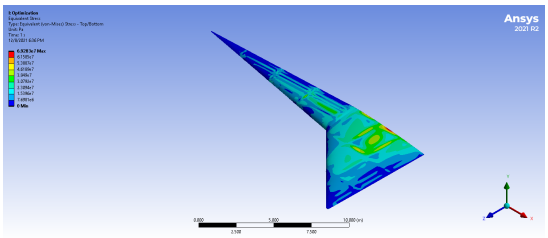

(b) Von Mises stress in optimized carbon fiber composite airframe

Figure 13: Results of simulated aerodynamic loading on a space plane wing. Have been optimized for weight and meet the requirements for stress and deflection outlined in Section 1

Once we had satisfied the design criteria at Max Q, we conducted the same analysis of both the carbon fiber and aluminum airframes at the other 7 altitudes and pressures. The results for these other analyses are presented in Appendix A and Appendix B.

5 Outcomes/Future Work

As a result of our mechanical loading simulations we successfully produced a wing design with the lowest mass possible that can support the mechanical loading caused by the shuttle re-entering the Earth's atmosphere. Through our analysis, we have determined that a carbon fiber composite wing would reduce the mass of the wing significantly while still meeting all load and deflection requirements. As shown in Table 2, even the optimized carbon fiber airframe was lighter than the optimized aluminum airframe. This is very significant result, due to the

importance of mass budgets in space flight. In fact, even at the highest stresses during reentry, our optimized design has a factor of safety of 6.5, which is well above NASA's requirements.

However, the carbon fiber airframe requires more careful analysis than the preliminary study done in this paper. Our study assumes that the carbon fiber layup produces isotropic material properties, but due to the nature of fiber-reinforced composites, it is likely that this is not the greatest approximation. Additionally, during design phases of a carbon fiber wing, the layup schedule will likely be designed to reinforce some areas more heavily than others. As a result, these results should be taken only as preliminary approximations, and not final results.

Additionally, it will be worth while to conduct the CFD analysis of turbulent flow mentioned in Section 3.2. This will allow much more accurate estimates of the aerodynamic loads on the wing. While the method used to approximate the top of wing pressures provides a reasonable order of magnitude estimate, it is still a very rough approximation.

Table 2: Summary of the mass of one wing made out of either Aluminum or Carbon Fiber Composite. The original passing geometry was the first geometry that passed the FoS & wing deflection requirements, while the optimized geometry was the lowest mass configuration that still met those operating requirements.

Material	Original Passing Geometry (kg)	Optimized Geometry (kg)
Aluminum	10,772	6,477.4
Carbon Fiber Composite	6,032.5	4,066.3

As mentioned at the end of Section 4.1, making the TPS out of ZrB_2 is not at all feasible. The reason we originally chose to use this ceramic, was because of the availability of data on it. Of the UHTCs that exist, ZrB_2 is one of the earliest and well-developed, so there is literature documenting all of its thermal properties. This area of research, however, is growing immensely, with new materials being developed all the time. We originally found one UHTC, $(Hf_{1/3}Ta_{1/3}Nb_{1/3})C$, which has a thermal conductivity of only 0.098 W/(m·K), and a density of 1.17 g/cm^3 [17]. If the TPS tiles were made out of this UHTC, using the 1D hand calculation listed in Eqn. 8, we get thicknesses on the order of a few millimeters, instead of almost a meter. In addition to just reduced thickness, we also get a huge decrease in the mass because the density is so much lower.

The reason why we did not use this material, however, is because it is such a new material, all of its properties are not yet known. So far, we know the density and thermal conductivity, but there have not been any studies on its specific heat, so we were unable to perform the analysis with it. As this material becomes more well-developed, along with others that are in similar stages, we expect to have many more options for creating the TPS. All together, with both the thermal and mechanical simulations and optimizations we have performed, we are well on our way to an improved shuttle wing design that could be used for a next gen space plane.

References

[1] National Aeronautics And Space Administration, *Wings in Orbit: Scientific and Engineering Legacies of the Space Shuttle, 1971-2010.* Place of publication not identified: U S Govt. Printing Office, 2011, OCLC: 942050897, ISBN: 978-0-16-086847-4.

[2] D. Adler, N. 12, and 2020. "Why did NASA retire the space shuttle?" Astronomy.com. (), [Online]. Available: https://astronomy.com/news/2020/11/why-did-nasa-retire-the-space-shuttle (visited on 11/17/2021).

[3] A. Pirolini. "Materials used in space shuttle thermal protection systems," AZO Materials. Section: Materials Article. (Oct. 9, 2014), [Online]. Available: https://www.azom.com/article.aspx?ArticleID=11443 (visited on 11/17/2021).

[4] Federal Aviation Administration. "Advanced aerospace medicine online: 4.1.7 returning from space." Last Modified: 2018-04-11T12:04:45-0400. (), [Online]. Available: https://www.faa.gov/about/office_org/headquarters_offices/avs/offices/aam/cami/library/online_libraries/aerospace_medicine/tutorial/section3/spacecraft_design/ (visited on 11/17/2021).

[5] Office of the Chief Engineer, *NASA-STD-5001b structural design and test factors of safety for spaceflight hardware*, Apr. 4, 2016. [Online]. Available: https://standards.nasa.gov/standard/nasa/nasa-std-5001 (visited on 11/16/2021).

[6] W. C. Rochelle, B. B. Roberts, L. D'Attorre, and M. A. Bilyk, "Shuttle orbiter re-entry flowfields at high angle of attack," *Journal of Spacecraft and Rockets*, vol. 10, no. 12, pp. 783–789, Dec. 1973, ISSN: 0022-4650, 1533-6794. DOI: 10.2514/3.61969. [Online]. Available: https://arc.aiaa.org/doi/10.2514/3.61969 (visited on 11/23/2021).

[7] NASA Johnson Space Center. "Shuttle (high res)." (Apr. 12, 2010), [Online]. Available: https://nasa3d.arc.nasa.gov/detail/shuttle-hi-res (visited on 11/23/2021).

[8] NASA Administrator. "Recordation drawings," NASA. Publisher: Brian Dunbar. (Jun. 5, 2013), [Online]. Available: http://www.nasa.gov/agency/crm/shuttle/drawings.html (visited on 11/23/2021).

[9] W. L. Ko and R. A. Fields, "Thermal stress analysis of space shuttle orbiter subjected to reentry aerodynamic heating," H-1400, Oct. 1, 1987, NTRS Author Affiliations: NASA Hugh L. Dryden Flight Research Center NTRS Document ID: 19880001007 NTRS Research Center: Legacy CDMS (CDMS). [Online]. Available: https://ntrs.nasa.gov/citations/19880001007 (visited on 11/23/2021).

[10] H. Yuan, J. Li, Q. Shen, and L. Zhang, "Preparation and thermal conductivity characterization of ZrB2 porous ceramics fabricated by spark plasma sintering," *International Journal of Refractory Metals and Hard Materials*, Special Section: Recent Advances of Functionally Graded Hard Materials, vol. 36, pp. 225–231, Jan. 1, 2013, ISSN: 0263-4368. DOI:

10.1016/j.ijrmhm.2012.09.003. [Online]. Available: https://www.sciencedirect.com/science/article/pii/S0263436812001709 (visited on 12/08/2021).

[11] L. Gong, W. Ko, and R. Quinn, "Thermal response of space shuttle wing during reentry heating," presented at the 19th Thermophysics Conference, NASA, Jun. 1984, p. 1761.

[12] Boeing. "Boeing: 787 by design: By design: Advanced composite use." (), [Online]. Available: https://www.boeing.com/commercial/787/by-design/#/advanced-composite-use (visited on 11/23/2021).

[13] "SHELL181." (), [Online]. Available: https://www.mm.bme.hu/~gyebro/files/ans_help_v182/ans_elem/Hlp_E_SHELL181.html (visited on 12/09/2021).

[14] P. Tranchard, S. Duquesne, F. Samyn, B. Estèbe, and S. Bourbigot, "Kinetic analysis of the thermal decomposition of a carbon fibre-reinforced epoxy resin laminate," *Journal of Analytical and Applied Pyrolysis*, vol. 126, pp. 14–21, Jul. 1, 2017, ISSN: 0165-2370. DOI: 10.1016/j.jaap.2017.07.002. [Online]. Available: https://www.sciencedirect.com/science/article/pii/S0165237017304163 (visited on 12/04/2021).

[15] J. C. Adams Jr., *Atmospheric re-entry*, Jun. 2003. [Online]. Available: https://engineering.purdue.edu/AAE450s/trajectories/Atmospheric%20Re-Entry.pdf (visited on 12/05/2021).

[16] J. M. Chen and C.-H. Liu, "Vortex shedding and surface pressures on a square cylinder at incidence to a uniform air stream," *International Journal of Heat and Fluid Flow*, vol. 20, no. 6, pp. 592–597, 1999. DOI: 10.1016/s0142-727x(99)00047-8.

[17] Z. Wu, X. Liang, Z. Shao, H. Chen, J. Li, and J. Wang, "Highly porous multicomponent (hf1/3ta1/3nb1/3)c ultra-high temperature ceramic with low thermal conductivity," *Materialia*, vol. 18, p. 101 158, Aug. 1, 2021, ISSN: 2589-1529. DOI: 10.1016/j.mtla.2021.101158. [Online]. Available: https://www.sciencedirect.com/science/article/pii/S2589152921001617 (visited on 11/23/2021).

A Analysis of Aluminum Airframe at 8 altitudes over reentry

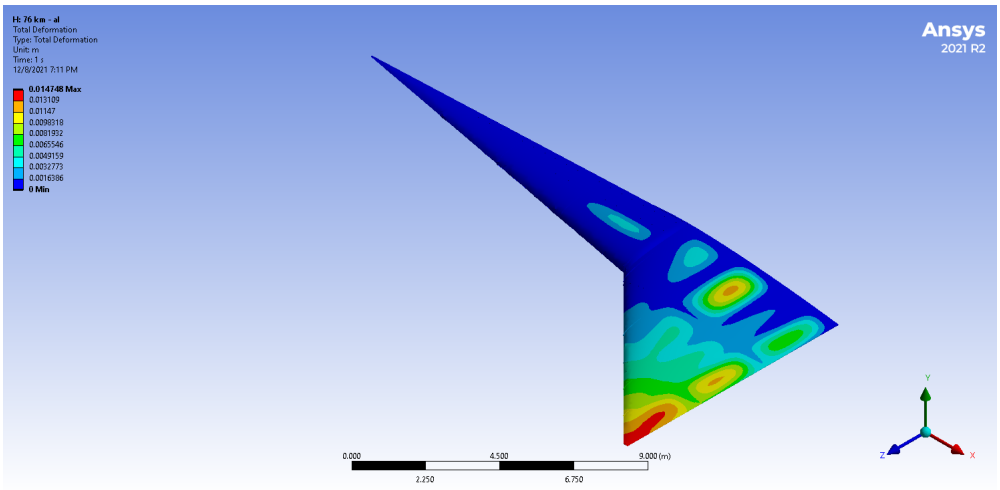

Figure 14: 76 km

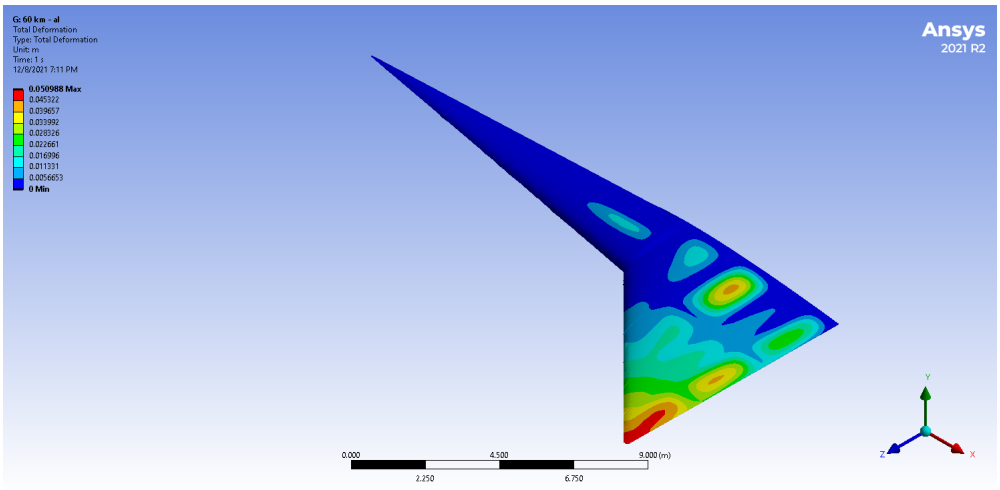

Figure 15: 60 km

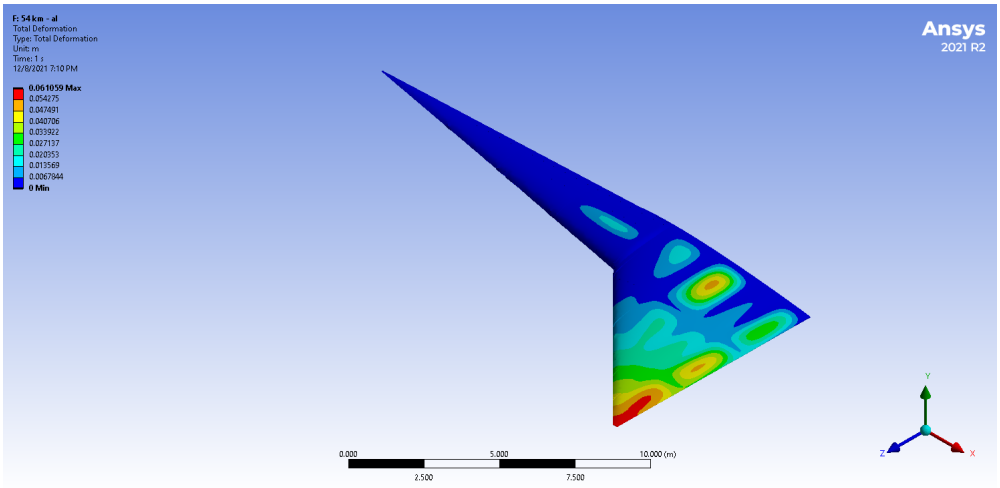

Figure 16: 54 km

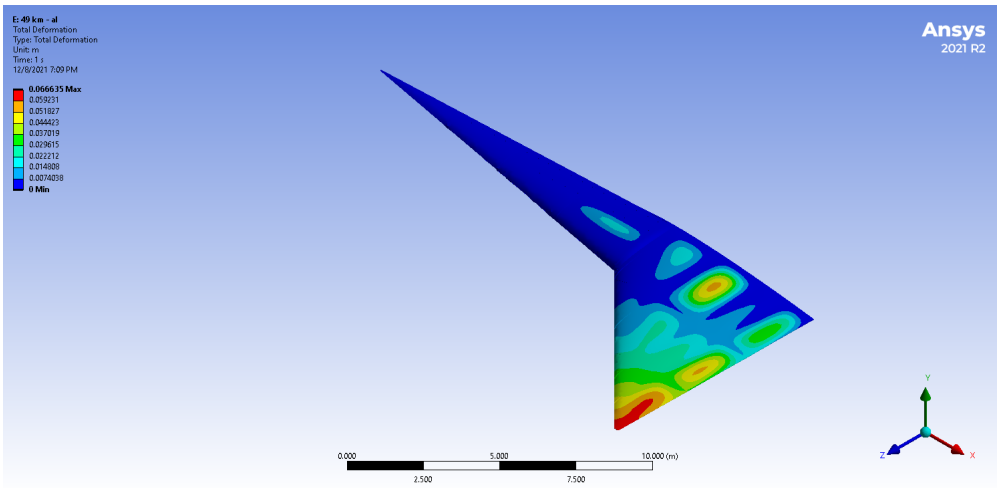

Figure 17: 49 km

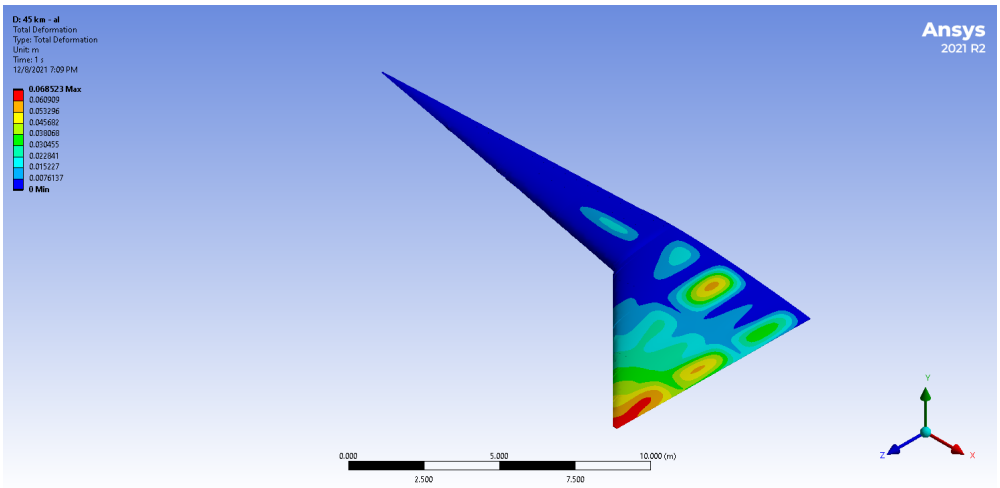

Figure 18: 45 km

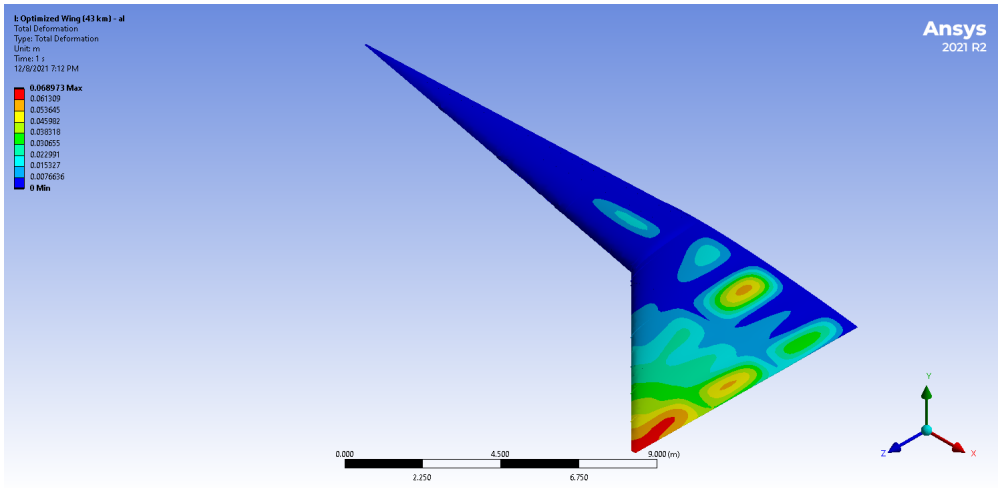

Figure 19: 43 km

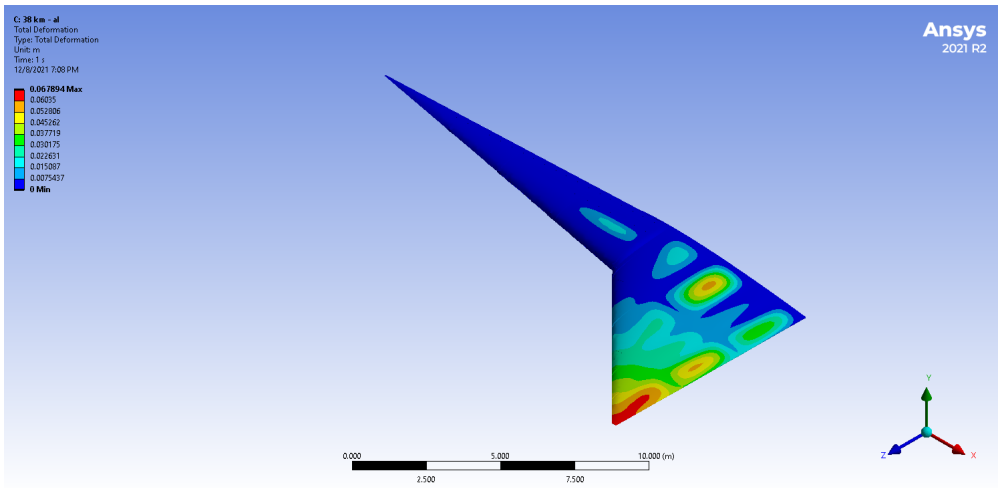

Figure 20: 38 km

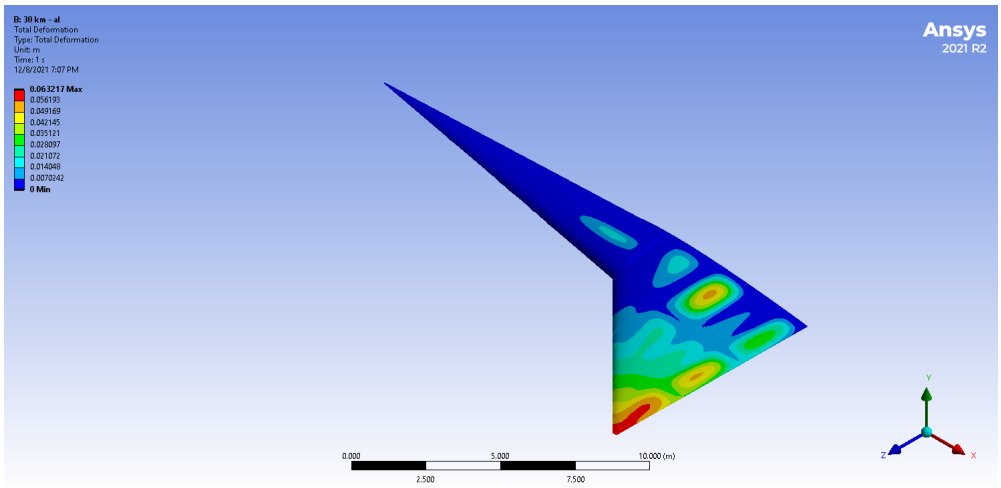

Figure 21: 30 km

B Analysis of Carbon Fiber Airframe at 8 altitudes over reentry

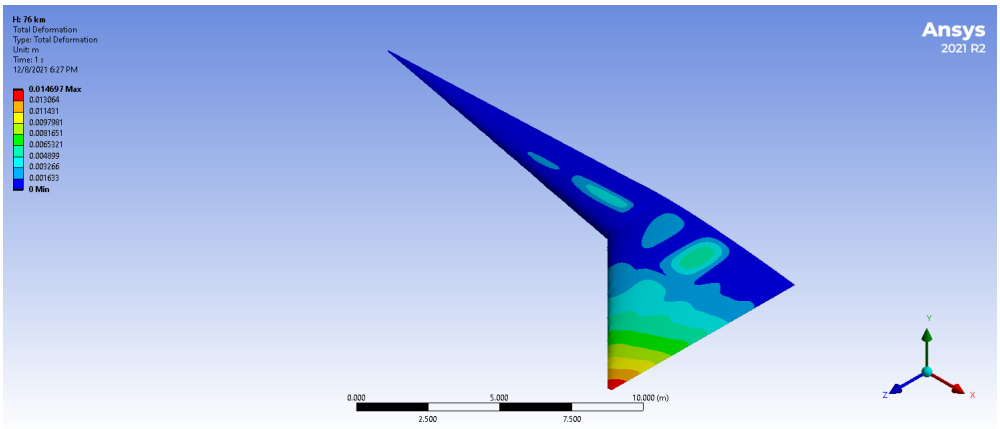

Figure 22: 76 km

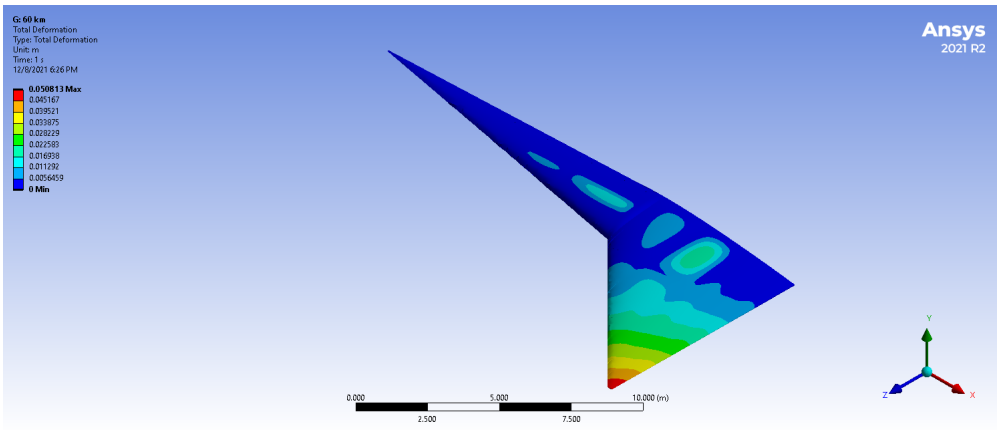

Figure 23: 60 km

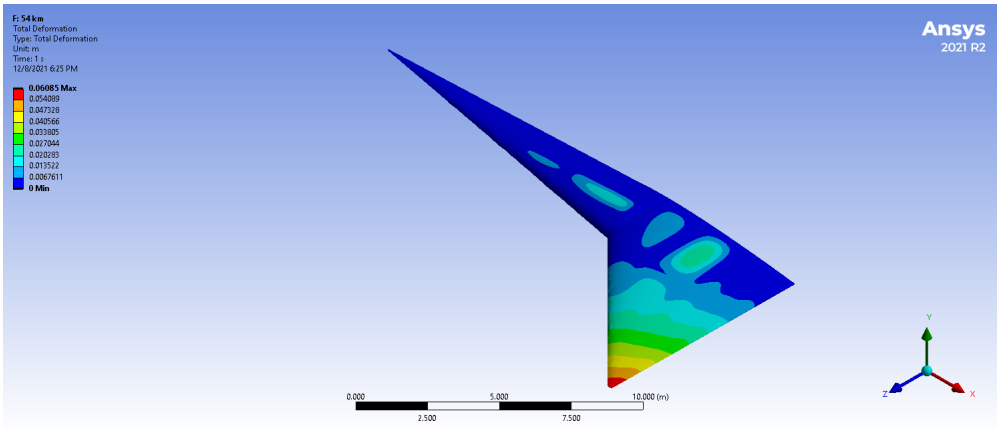

Figure 24: 54 km

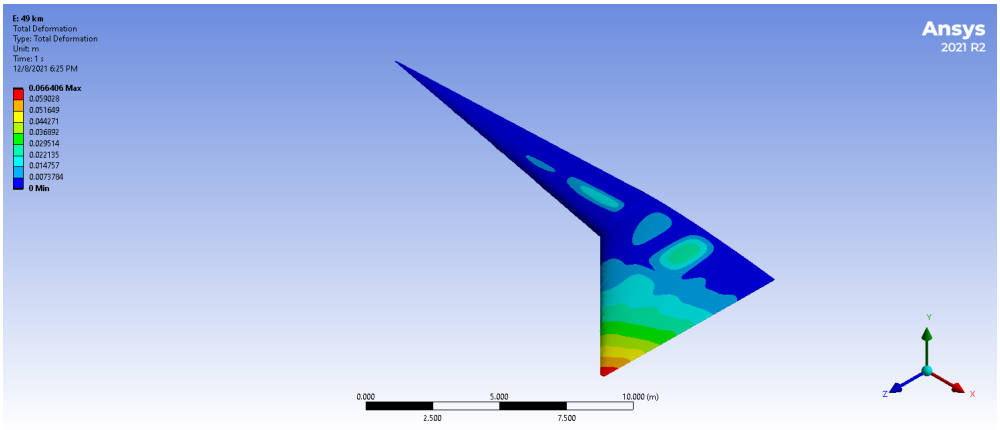

Figure 25: 49 km

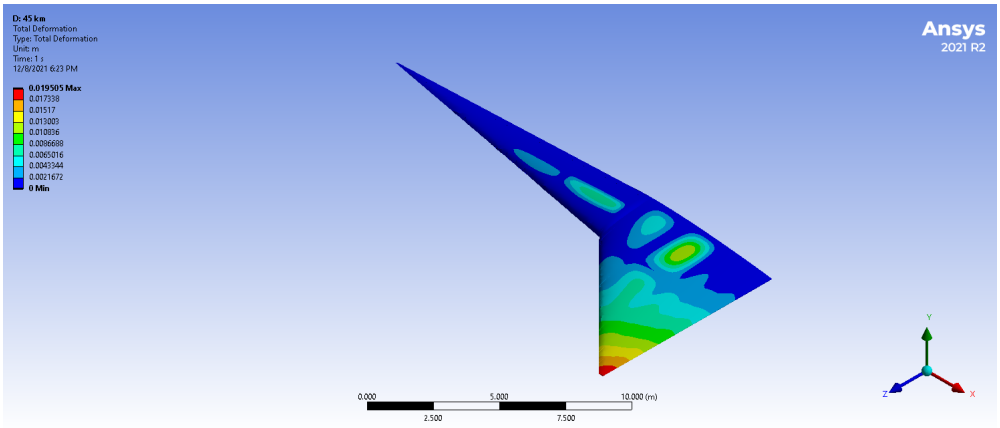

Figure 26: 45 km

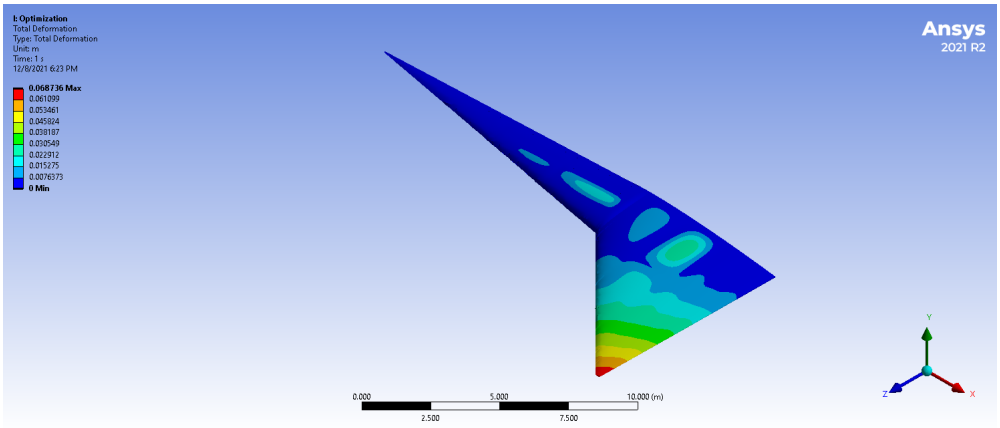

Figure 27: 43 km

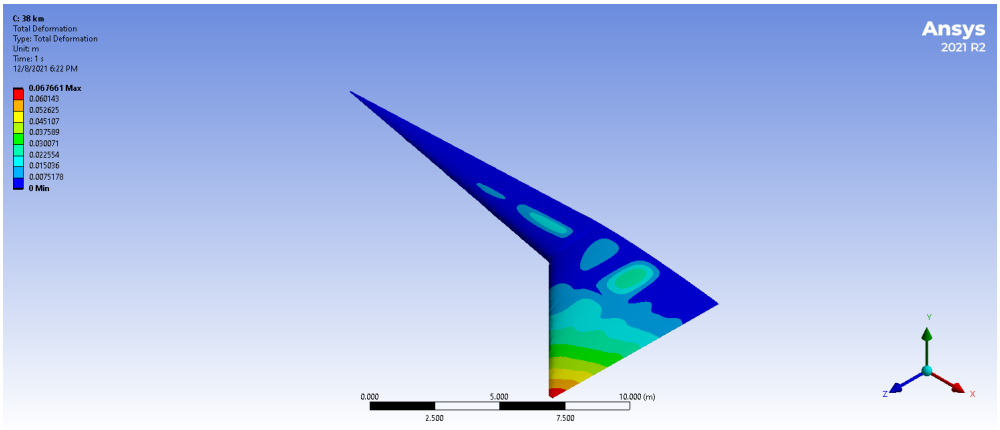

Figure 28: 38 km

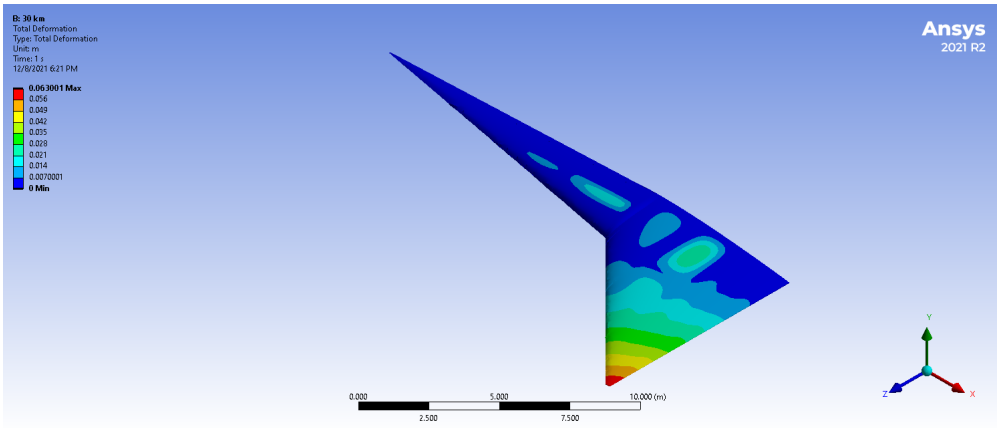

Figure 29: 30 km